Low-complexity Adaptive Broadband Beamforming Based on the Non-uniform Decomposition Method

Shurui Zhang[a,b], Jeyarajan Thiyagalingam[c], Weixing Sheng[a,*], Thia Kirubarajan[b], Xiaofeng Ma[a]

[a] *School of Electronic and Optical Engineering, Nanjing University of Science and Technology, Nanjing, China*
[b] *Department of Electrical and Computer Engineering, McMaster University, Hamilton, Canada*
[c] *Department of Electrical Engineering and Electronics, University of Liverpool, Liverpool, United Kingdom*

Abstract

Sub-band adaptive processing is an established method to design a broadband beamformer. The uniform decomposition method (UDM) is a common approach for designing sub-band adaptive beamformer (SAB) that would split the received signal into a number of uniform sub-bands. However, the UDM has redundancies on decomposed sub-bands at high frequencies in the passband. In this paper, we propose a number of techniques to overcome this issue. By proposing a novel relative bandwidth method (RBM), we obtain that the relative bandwidth of each sub-band is the same. Using this as a basis, we present a non-uniform decomposition method (NUDM) such that the NUDM has fewer sub-bands than the conventional UDM, leading to reduced computational complexity. We also propose an elegant metric, adjacent bandwidth ratio (ABR), to facilitate easier comparison of non-uniformity. We then extend NUDM method to provide a fast variant of the non-uniform decomposition SAB (FNUD-SAB). We ensure that the sub-band frequencies and corresponding adaptive weights are available as part of the proposed FNUD-SAB method. With undistorted response to the desired signal and effective anti-jamming capability, the new beamformer reduces the computational complexity by reducing the number of sub-bands. Simulation results highlight the effectiveness of the proposed methods.

Keywords: Broadband beamforming; Sub-band adaptive beamformer; Uniform decomposition method; Non-uniform decomposition

1. Introduction

Adaptive broadband beamforming has been an important topic of research over the past few decades because of its extensive applications in various fields, such as radar, sonar, microphone arrays, medical imaging, seismology, astronomy and radio communications [1, 2, 3, 4]. Adaptive broadband beamforming techniques can be categorized into two major groups, namely, space-time beamforming and sub-band beamforming [1].

In space-time beamforming, the broadband property of the array is achieved by processing the received signal of each antenna with appropriate temporal-domain filters, such as finite impulse response (FIR) filters [5], infinite impulse response (IIR) filters [6, 7, 8], and Laguerre filters [9]. Because of its effectiveness and simplicity, space-time processing is commonly used to implement broadband beamforming. However, space-time methods have a

*Corresponding author
Email address: shengwx@njust.edu.cn (Weixing Sheng)

high computational complexity for broadband scenarios with a large number of sensors and correspondingly wider bandwidth, making the length of the space-time filters large [3]. To implement an adaptive broadband beamformer with effective interference rejection capability and high angular resolution, arrays with a large number of sensors and filter coefficients have to be employed [10]. Although algorithms have been proposed in [11, 12] to reduce the computational complexity of space-time methods, the beamformer still has large computational burden with a large number of sensors and the wide bandwidth. Therefore, the space-time beamforming has a high computational complexity, especially when the scale of the array is large and the bandwidth is wide.

The alternative to adaptive broadband beamforming is the sub-band adaptive beamforming (SAB) [1]. The SAB uses a filter bank to split each input signal into a set of distinct frequency signal components, each covering a fraction of the input signal bandwidth, and then used individually in beamforming. The basic idea behind SAB is to first split the received sensor signals into uniform sub-bands and then operate an independent beamformer in each of them, with the sub-band beamformer being selected based on the specific applications [1]. The SAB provides an efficient divide-and-conquer technique using a set of parallel and smaller sub-band adaptive beamformers [13]. Since various sub-band decomposition techniques can be employed in the beamforming process to improve performance with the wide bandwidth of the received array signal [1], the SAB has more practical applications than the space-time beamforming. Sub-band methods to adaptive beamforming have been widely used in microphone and antenna arrays [1, 14, 15, 16, 17, 18, 19, 20, 21, 22].

In generally, the conventional SAB, the passband is decomposed into uniform sub-bands, and hence the name: uniform decomposition SAB (UD-SAB). As such, each sub-band has the same absolute bandwidth and results in redundancies on divided sub-bands at high frequencies in the passband. In this paper, we propose an approach where each sub-band have the same relative bandwidth opposed to absolute bandwidth. In other words, the higher frequency sub-band will have a larger absolute bandwidth than a sub-band in the lower frequency end. Building on the proposed relative bandwidth method (RBM), we develop a non-uniform decomposition method (NUDM), that splits the passband into a number of non-uniform sub-bands, yet their relative bandwidths being the same. As discussed in the latter part of this paper, this reduces the total number of sub-bands, and associated computations, and hence the computational complexity of the overall beamforming process. We extend the proposed NUDM approach even further to realize an accelerated version of the NUDM, which we refer to as fast non-uniform decomposition sub-band beamformer (FNUD-SAB). Similar to the UD-SAB, the FNUD-SAB uses the fast Fourier transform (FFT) and the inverse FFT (IFFT) as the analysis and synthesis filters, providing quick and effective means for transforming the signals between temporal and frequency domains. The proposed FNUD-SAB reduces the computational complexity by effectively reducing the number of sub-bands, which are needed to calculate the adaptive weight vectors. However, the NUDM ensures that the FNUD-SAB yields undistorted response to signal of interest (SOI) and restrained responses to interference signals. To facilitate easier comparison of these beamforming methods, we propose a simple yet elegant metric, known as adjacent bandwidth ratio (ABR), to quantify and compare different methods. As such, we make the following key contributions in this paper:

1. We propose a relative bandwidth method (RBM) that decouples the relationship between the relative bandwidth of a sub-band and its center frequency;

2. We present a novel, non-uniform decomposition method (NUDM) based on RBM. The proposed method reduces the number of sub-bands, and thereby reduced the overall computational complexity of the sub-band processing;
3. We built and provide an implementation of a fast version of the NUD-SAB (FNUD-SAB). This FNUD-SAB has fewer sub-bands than the uniform decomposition sub-band adaptive beamformer (UD-SAB); and
4. We propose a novel adaptive implementation of the FNUD-SAB to overcome the numerical instability arising out of the fact that non-uniform discrete Fourier transform being ill-conditioned for a large number of elements.

The rest of this paper is organized as follows: In Section 2, we discuss the relative bandwidth method (RBM) in detail, which is then followed by Section 3, where we propose the NUDM in detail. In Section 4, the structure of the FNUD-SAB and its adaptive implementation are given. In Section 5, we present the results of our detailed simulation studies and we highlight the effectiveness of the proposed method. We also analyze the computational complexity of the proposed algorithm against the baseline version. We finally conclude the paper in Section 6. Throughout this paper, we use a number of abbreviations which are listed in Table 1 below.

Table 1: The abbreviations in this paper

SAB	Sub-band adaptive beamformer	RBM	Relative bandwidth method
UDM	Uniform decomposition method	NUDM	Non-uniform decomposition method
UD-SAB	Uniform decomposition SAB	FNUD-SAB	Fast non-uniform decomposition SAB
FIR	Finite impulse response	IIR	Infinite impulse response
FFT	Fast Fourier transform	IFFT	Inverse FFT
SOI	Signal of interest	ULA	Uniform linear array
DFT	Discrete Fourier transform	DOA	Direction of arrival
NDFT	Non-uniform discrete Fourier transform	NIDFT	Non-uniform inverse discrete Fourier transform
ABR	Adjacent bandwidth ratio	SIR	Signal-to-interference ratio
INR	Interference-to-noise ratio	SINR	Signal-to-interference-to-noise ratio

2. Relative Bandwidth Method

In this section, the RBM, which proves that the relative bandwidth of each sub-band is the same in the SAB, is proposed. The RBM is important in analyzing the properties of the NUDM and FNUD-SAB. A uniform linear array (ULA) with M antennas is assumed for the SAB, and all of the sensors are omnidirectional with the same response. In the following, d is the distance between two elements of the ULA as shown in Fig. 1. In order to avoid the grating lobes, d is equal to half the wavelength of the maximum frequency. Assume that the signals impinge upon the array from the far field. The received signal is decomposed into K sub-bands, and f_k is the

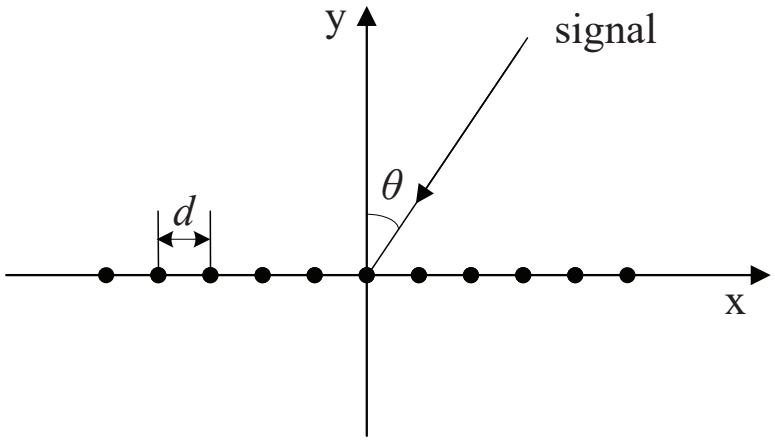

Figure 1: Uniform linear array with a sensor spacing of d, where the signal impinges from the direction θ.

centre frequency of the k-th sub-band. Also, c is the speed of light in free space, θ is the direction of arrival (DOA), and θ_0 is the direction of SOI. The core idea of the sub-band beamforming is that the broadband processing is split into narrowband processing, and each sub-band beamforming should meet the narrowband beamforming. Therefore, the normalization gain of the k-th sub-band is given by [23]

$$\begin{aligned} G_k(f,\theta) &= \tfrac{1}{M^2}\left|\sum_{m=1}^{M} e^{j2\pi(m-1)\frac{d}{c}(f\sin\theta - f_k\sin\theta_0)}\right|^2 \\ &= \tfrac{1}{M^2}\left|\frac{1-e^{j2\pi M\frac{d}{c}(f\sin\theta - f_k\sin\theta_0)}}{1-e^{j2\pi\frac{d}{c}(f\sin\theta - f_k\sin\theta_0)}}\right|^2 \\ &= \tfrac{1}{M^2}\left|\frac{e^{j\pi M\frac{d}{c}(f\sin\theta - f_k\sin\theta_0)}\left[e^{-j\pi M\frac{d}{c}(f\sin\theta - f_k\sin\theta_0)} - e^{j\pi M\frac{d}{c}(f\sin\theta - f_k\sin\theta_0)}\right]}{e^{j\pi\frac{d}{c}(f\sin\theta - f_k\sin\theta_0)}\left[e^{-j\pi\frac{d}{c}(f\sin\theta - f_k\sin\theta_0)} - e^{j\pi\frac{d}{c}(f\sin\theta - f_k\sin\theta_0)}\right]}\right|^2 \\ &= \tfrac{1}{M^2}\left|e^{j\pi(M-1)\frac{d}{c}(f\sin\theta - f_k\sin\theta_0)}\right|^2\left|\frac{\sin[\pi M\frac{d}{c}(f\sin\theta - f_k\sin\theta_0)]}{\sin[\pi\frac{d}{c}(f\sin\theta - f_k\sin\theta_0)]}\right|^2 \\ &= \left|\frac{\sin[\pi M\frac{d}{c}(f\sin\theta - f_k\sin\theta_0)]}{M\sin[\pi\frac{d}{c}(f\sin\theta - f_k\sin\theta_0)]}\right|^2 \end{aligned} \tag{1}$$

where f denotes the frequency, which is received and processed by the k-th sub-band. With

$$f_k\sin\theta_0 = f\sin\theta \tag{2}$$

$G_k(f,\theta)$ attains the maximum value. It is assumed that Δf_k and $\Delta\theta$ are the offsets in the frequency and DOA, respectively. That is, $f = f_k + \Delta f_k$ and $\theta = \theta_0 + \Delta\theta$. Then,

$$\begin{aligned} f_k\sin\theta_0 &= (f_k+\Delta f_k)\sin(\theta_0+\Delta\theta) \\ &= f_k\sin\theta_0\cos\Delta\theta + f_k\cos\theta_0\sin\Delta\theta + \Delta f_k\sin\theta_0\cos\Delta\theta + \Delta f_k\cos\theta_0\sin\Delta\theta \end{aligned} \tag{3}$$

Since Δf_k and $\Delta\theta$ are assumed to be small, $\cos\Delta\theta \approx 1$, $\sin\Delta\theta \approx \Delta\theta$ and $\Delta\theta\Delta f_k \approx 0$. Than, (3) can be rewritten as

$$f_k\sin\theta_0 = f_k\sin\theta_0 + \Delta\theta f_k\cos\theta_0 + \Delta f_k\sin\theta_0 \tag{4}$$

Also, (4) can be rewritten as

$$\Delta\theta = -\frac{\Delta f_k\sin\theta_0}{f_k\cos\theta_0} = -\frac{\Delta f_k}{f_k}\tan\theta_0 \quad \text{(rad)} \tag{5}$$

Note that (5) indicates that, if the k-th sub-band beamformer uses the signal $f = f_k + \Delta f_k$ for beamforming, the beam pattern has the look direction error $\Delta\theta$, which is negatively correlated with Δf_k. If $f > f_k$, indicating that Δf_k is positive-real, the actual look direction is smaller than the direction of SOI. Conversely, if $f < f_k$, indicating that Δf_k is negative-real, the actual look direction is larger than the direction of SOI.

The mainlobe width increases with increasing SOI [23]. To ensure satisfactory performance of the phased array, the range of scanning angles are $\pm 60°$ [23]. When $\theta_0 = 60°$, (5) can be rewritten as

$$\Delta\theta = -\frac{\sqrt{3}\Delta f_k}{f_k} \qquad \text{(rad)} \tag{6}$$

The peak frequency deviation of the k-th sub-band is assumed to be Δf_k. Then, the bandwidth of the k-th sub-band is obtained as $B_k = 2\,|\Delta f_k|$. Based on (6), the relative bandwidth ΔB_k of the k-th sub-band is obtained as

$$\Delta B = \Delta B_k = \frac{B_k}{f_k} = \frac{2\Delta\theta}{\sqrt{3}} \tag{7}$$

Note that (7) indicates that the relative bandwidth of each sub-band is the same and is only a function of the look direction error $\Delta\theta$, i.e., it has no relationship to the centre frequency. The pointing error should be in the range of the half-power beamwidth (3dB beamwidth) [23]. An approach to obtain the half of 3dB beamwidth $\theta_{0.5}$ is discussed below.

Based on (1), when the frequency of the received signal is $\hat{f}$, the half-power gain can be obtained as

$$\left| \frac{\sin[\pi M \frac{d\hat{f}}{c}(\sin\hat{\theta} - \sin\theta_0)]}{M \sin[\pi \frac{d\hat{f}}{c}(\sin\hat{\theta} - \sin\theta_0)]} \right|^2 = 0.5 \tag{8}$$

where $\hat{\theta}$ is the DOA and has the half-power gain. For simplicity, assume that $\hat{\theta} > \theta_0$. Since $\hat{\theta}$ is close to θ_0, $\sin\hat{\theta} - \sin\theta_0 \approx 0$ and $\sin[\pi \frac{d\hat{f}}{c}(\sin\hat{\theta} - \sin\theta_0)] \approx \pi \frac{d\hat{f}}{c}(\sin\hat{\theta} - \sin\theta_0)$. Thus, (8) can be rewritten as

$$\frac{\sin[\pi M \frac{d\hat{f}}{c}(\sin\hat{\theta} - \sin\theta_0)]}{\pi M \frac{d\hat{f}}{c}(\sin\hat{\theta} - \sin\theta_0)} = \frac{1}{\sqrt{2}} \tag{9}$$

The left-hand side of (9) is the sinc function. Thus,

$$\pi M \frac{d\hat{f}}{c}(\sin\hat{\theta} - \sin\theta_0) = 1.39 \tag{10}$$

(10) can rewrite as

$$2\sin[\frac{(\hat{\theta} - \theta_0)}{2}]\cos[\frac{(\hat{\theta} + \theta_0)}{2}] = \frac{1.39c}{\pi M d\hat{f}} \tag{11}$$

Since $\hat{\theta} \approx \theta_0$, $\cos[\frac{(\hat{\theta}+\theta_0)}{2}] \approx \cos\theta_0$ and $\sin[\frac{(\hat{\theta}-\theta_0)}{2}] \approx \frac{(\hat{\theta}-\theta_0)}{2}$, and the half of 3dB beamwidth of $\hat{f}$ is $\theta_{0.5}(\hat{f}) = \hat{\theta} - \theta_0$, the left-hand side of (11) can be obtained as

$$2\sin[\frac{(\hat{\theta} - \theta_0)}{2}]\cos[\frac{(\hat{\theta} + \theta_0)}{2}] \approx \theta_{0.5}(\hat{f})\cos\theta_0 \tag{12}$$

From (11) and (12), the half of 3dB beamwidth $\theta_{0.5}(\hat{f})$ is obtained as

$$\theta_{0.5}(\hat{f}) = \frac{1.39c}{\pi M d\hat{f}\cos\theta_0} \qquad \text{(rad)} \tag{13}$$

As given by (13), with the decrease in $|\theta_0|$ and the increase in frequency $\hat{f}$, the half of 3dB beamwidth increases gradually. To ensure accurate beam pointing, the minimun half of 3dB beamwidth of the passband frequency should be regarded as the half of 3dB beamwidth of the beamformer. In that case, $\theta_0 = 0°$ and $\hat{f}$ is equal to the maximum frequency of the passband $f_{\max}$. Therefore, the half of 3dB beamwidth $\theta_{0.5}$ is obtained as

$$\theta_{0.5} = \frac{1.39c}{\pi M d f_{\max}} \qquad \text{(rad)} \tag{14}$$

As discussed after (7), acceptable pointing error is in the range of half-power beamwidth. Therefore, $\Delta\theta = \theta_{0.5}$, and rewrite (7) as

$$\Delta B = \frac{2.78c}{\sqrt{3}\pi M d f_{\max}} \tag{15}$$

With $d = \frac{c}{2f_{\max}}$, (15) can be rewritten as

$$\Delta B = \frac{5.56}{\sqrt{3}\pi M} \tag{16}$$

3. Non-uniform Decomposition Method

To guarantee an acceptable look direction error, each sub-band should conform to the RBM in (16). The UDM is commonly used to decompose the passband for the SAB. The sub-band with the lowest centre frequency has the lowest absolute bandwidth. Therefore, in the UDM, the lowest absolute bandwidth of sub-bands should be used to decompose the passband uniformly, as shown in Fig. 2(a).

As can be observed in (16), the relative bandwidth of a sub-band has no relationship with its center frequency. In the same relative bandwidth, the higher frequency sub-bands have correspondingly larger absolute bandwidths. If the NUDM satisfying the RBM in (16) is used to decompose the passband, the new decomposition method has fewer sub-bands than the UDM, especially in the large passband case. In this section, a new method, NUDM, is proposed to reduce the number of sub-bands. With fewer sub-bands, the computational complexity of the frequency sub-band adaptive approach is correspondingly reduced.

Assume that the passband is decomposed into K non-uniform sub-bands, and that the maximum and minimum frequencies of the k-th sub-band are $\bar{f}_k$ and $\bar{f}_{k-1}$, respectively. Thus, the $K+1$ boundary frequencies of the sub-bands are $\bar{f}_k,\ k = 0, 1, ..., K$, where $\bar{f}_0$ and $\bar{f}_K$ are the minimum and maximum frequencies of the passband, respectively. The centre frequency of the k-th sub-band is

$$f_k = \frac{\bar{f}_k + \bar{f}_{k-1}}{2} \tag{17}$$

The relative bandwidth of the k-th sub-band is

$$\frac{\left(\bar{f}_k - \bar{f}_{k-1}\right)}{\left(\frac{\bar{f}_k + \bar{f}_{k-1}}{2}\right)} = \Delta B \tag{18}$$

Then, (18) is rewritten as

$$\bar{f}_k = \left(\frac{2 + \Delta B}{2 - \Delta B}\right) \bar{f}_{k-1} \tag{19}$$

where $k = 1, 2, ..., K$. Assume $q = \left(\frac{2+\Delta B}{2-\Delta B}\right)$. Since $\Delta B > 0$, $q > 1$. (19) can be rewritten as $\bar{f}_k = q\bar{f}_{k-1}$, $k = 1, 2, ..., K$, which indicates that the boundaries of the sub-bands follow a geometric series. Assume that $f_{\min}$ is the lowest frequency of the passband and $\bar{f}_0 = f_{\min}$. Then, the highest frequency of the k-th sub-band, $\bar{f}_k$, is

$$\bar{f}_k = q^k f_{\min} \qquad (k = 1, 2, ..., K) \tag{20}$$

From (17) and (20), the center frequency of the k-th sub-band f_k is

$$f_k = \frac{(q+1)f_{\min}}{2} q^{k-1} = f_1 q^{k-1} \tag{21}$$

where $k = 1, 2, ..., K$. As indicated in (21), when the relative bandwidths of the sub-bands are the same, the centre frequencies of those sub-bands also follow a geometric series.

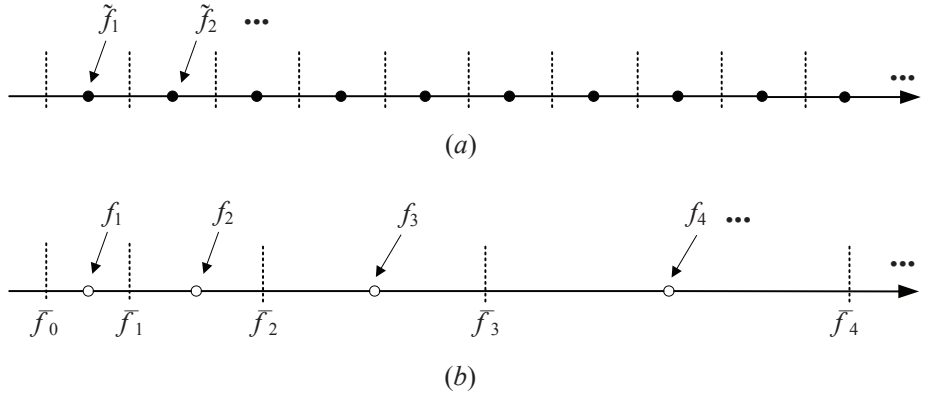

Figure 2: Schematic diagram of (a) uniform and (b) non-uniform sub-band decomposition methods.

In order to make the look direction error in the range of half-power beamwidth, the decomposition of the sub-band should satisfy the RBM. As indicated by (16), the relative bandwidth of a sub-band has no relationship with its center frequency, and relative bandwidths of all sub-bands have the same value. The minimum absolute bandwidth is the first sub-band of the passband and should be satisfied in both the UDM and NUDM. In the conventional UDM, the minimum absolute bandwidth is used to decompose the passband. Since the absolute bandwidths of the sub-bands increase with the increase in the centre frequency, the NUDM can decompose passband with fewer sub-bands as shown in the schematic diagram in Fig. 2. Form (16) and (20), the number of the non-uniform sub-band using NUDM can be obtained as $\left\lceil \log_q^{\frac{f_{\max}}{f_{\min}}} \right\rceil$, where $\lceil \bullet \rceil$ is the ceiling operator which rounds up the given argument to the next integer. With the increase of the number of antennas, the relative bandwidth ΔB in (16) and the common ratio q in (19) will decrease in value. Therefore, when the passband width is the same, the beamformer with large number of antennas will entail additional sub-bands. In addition to this, if the passband width is increased while keeping the number of antennas a constant, the number of sub-bands will increase.

In this paper, a single-number metric, adjacent bandwidth ratio (ABR), is proposed for a simpler and more immediate comparison. In simple terms, since the UDM splits the passband into the uniform sub-bands, the ABR of the UDM is simply a unit value. In the case of NUDM, the bandwidths of the k-th and $(k-1)$-th sub-band

are

$$
\begin{aligned}
B_k &= \bar{f}_k - \bar{f}_{k-1} = q^k f_{\min} - q^{k-1} f_{\min} = q^{k-1} f_{\min}(q-1) \\
B_{k-1} &= \bar{f}_{k-1} - \bar{f}_{k-2} = q^{k-1} f_{\min} - q^{k-2} f_{\min} = q^{k-2} f_{\min}(q-1)
\end{aligned}
\tag{22}
$$

Thus, the ABR of the NUDM is equal to $\frac{B_k}{B_{k-1}} = q$. When the passband bandwidth is the same, a method, whose ABR q is much larger than one, has the lowest number of sub-bands. In other words, the method with the largest value of q has the lowest computational complexity.

4. Fast Non-uniform Decomposition Sub-band Adaptive Beamformer

As shown in (21), the non-uniform discrete Fourier transform (NDFT), whose sample frequencies match the NUDM, can be used to decompose the received signal for the SAB. However, the NDFT is expressed in a matrix form using a Vandermonde matrix [24], and for large values of K, the Vandermonde matrix is ill-conditioned (except when the NDFT reduces to the conventional Discrete Fourier transform, i.e., DFT). Thus, a direct inverse computation is not desirable [24].

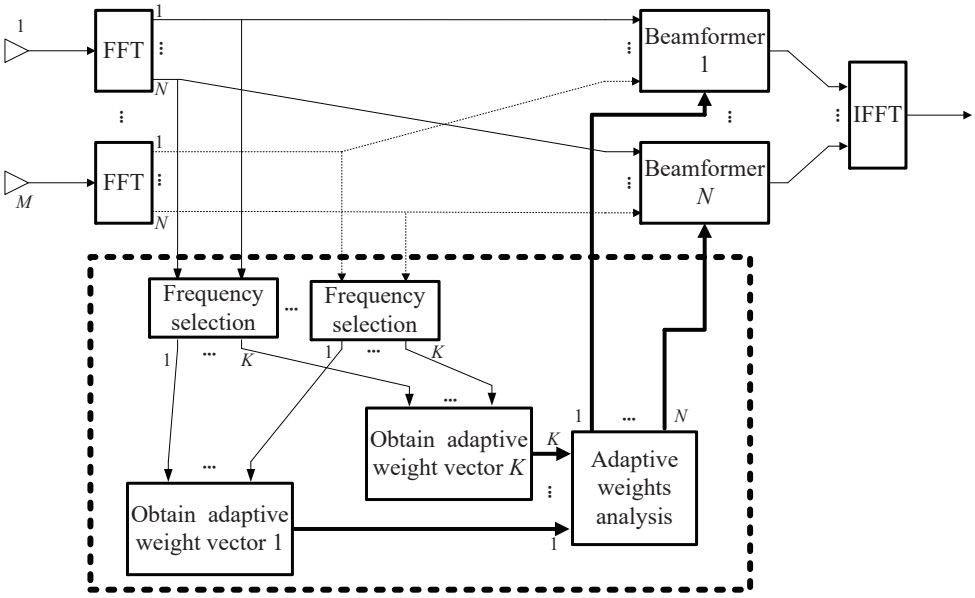

Figure 3: Fast non-uniform decomposition sub-band adaptive beamformer.

Using this as a motivation, in this section, a new SAB using UNDM is proposed as shown in Fig. 3. The analysis and synthesis filters use the classical structures, i.e., the FFT and IFFT. The analysis filters split each input signal into a set of frequency sub-bands, and each sub-band covers a fraction of the input signal bandwidth. Sub-band beamforming provides an efficient divide-and-conquer strategy using a set of parallel and smaller sub-band algorithms.

In many cases, the sub-band processing is performed together with decimation, which reduces the dimensionality of the data in the sub-band algorithm [13]. As highlighted before, the key focus of this paper is to reduce the number of sub-bands. With the UNDM proposed in Section 3, the flow of the frequency selection module, shown in Fig. 3, is provided in **Algorithm 1**. The passband is decomposed into N sub-bands uniformly by the

analysis filters, i.e., FFT. The centre frequency of each uniform sub-band is $\tilde{f}_n, (n = 1, 2, ..., N)$, and the required non-uniform centre frequencies are $f_k, (k = 1, 2, ..., K)$. As discussed at the end of Section 3, the NUDM can decompose the passband with fewer sub-bands than the uniform sub-band decomposition method, i.e., $K < N$.

Algorithm 1 NUDM Frequency Selection Module

1: Initialize: $f_1 = \tilde{f}_1$, $f'_2 = qf_1$ and $k = 2$

2: Obtain f_k:

$$\begin{cases} f_k = \underset{\tilde{f}_n}{\arg} \ \min \left| f'_k - \tilde{f}_n \right| \\ s.t \quad \tilde{f}_n < f'_k \end{cases} \tag{23}$$

3: $k = k + 1$ and $f'_k = qf_{k-1}$. If $f'_k > f_{\max}$, end loop; Else, jump to Step 2.

In **Algorithm 1**, the geometric sequence shown as (21) is used to find the frequency f'_k. In Step 2, $\tilde{f}_n$, which has the minimum distance with the f'_k and is smaller than f'_k, is chosen as the using of f_k satisfying RBM in (21). Otherwise, if $\tilde{f}_n > f'_k$ and $f_k = \tilde{f}_n$, one may obtain that $f_k > qf_{k-1}$, which dose not satisfy (21). Using NUDM, the **Algorithm 1** has fewer sub-bands than the UDM. Thus, the **Algorithm 1** has lower computational burden than the UDM. Moreover, the non-uniform frequencies can be obtained offline and the frequency selection modules only need to save the frequency, which should be used to calculate the adaptive weights. Since the frequency selection modules can be offline (not real-time), the proposed **Algorithm 1** does not increase computational complexity in real-time and simplifies implementation.

As illustrated in Fig. 3, the signal is decomposed into N uniform sub-bands via FFT. The frequency selection module reduces the number of sub-bands to K based on **Algorithm 1**. Using the frequency-domain constrained adaptive algorithm, the adaptive weights of those K sub-bands can be obtained. Sub-band algorithms are conventionally derived with the sub-band index as the center frequency, i.e., by treating each sub-band as independent from the others [13]. As illustrated in Fig. 3, the adaptive weight analysis modules yield the adaptive weights for N sub-bands. The frequency constrained adaptive algorithm of K selected sub-bands and the way to obtain the adaptive weights for the N sub-bands are discussed now.

Using the FFT and frequency selection module, the k-th sub-band input signal of the m-th sensor is denoted as $X_{k,m}$, and they are arranged as a vector as

$$\mathbf{X}_k = [X_{k,1}, X_{k,2}, ..., X_{k,M}]^T \tag{24}$$

where the superscript $[\bullet]^T$ denotes the matrix transpose, and $k = 1, 2, ..., K$. The frequency-domain constraint $\mathbf{c}_k$ and adaptive weights of k-th sub-band $\mathbf{w}_k$ are arranged as vectors as

$$\mathbf{c}_k = [e^{-j2\pi f_k \tau_1(\theta_0)}, e^{-j2\pi f_k \tau_2(\theta_0)}, ..., e^{-j2\pi f_k \tau_M(\theta_0)}]^T \tag{25}$$

and

$$\mathbf{w}_k = [w_{k,1}, w_{k,2}, ..., w_{k,M}]^T \tag{26}$$

In (25), $\tau_m = [(m-1)d \sin\theta_0]/c$. The adaptive beamforming weights of the k-th sub-band can be obtained

using the standard frequency-domain linearly constrained minimum variance (LCMV) algorithm [1, 25] as

$$\begin{cases} \min\limits_{\mathbf{w}_k} & \mathbf{w}_k^H \mathbf{R}_k \mathbf{w}_k \\ s.t. & \mathbf{c}_k^H \mathbf{w}_k = \mathbf{f}_k \end{cases} \tag{27}$$

In (27), $\mathbf{R}_k = E\{\mathbf{X}_k \mathbf{X}_k^H\}$ is the sub-band data correlation matrix and $\mathbf{f}_k$ is the distortionless response for the desired signal in the k-th sub-band. The optimum weight vector of the k-th sub-band $\mathbf{w}_{k,opt}$ is solved from (27) using the Lagrange multiplier method and is expressed as

$$\mathbf{w}_{k,opt} = \mathbf{R}_k^{-1} \mathbf{c}_k \left[\mathbf{c}_k^H \mathbf{R}_k^{-1} \mathbf{c}_k \right]^{-1} \mathbf{f}_k \tag{28}$$

In real-time scenarios, the adaptive weights can be obtained iteratively [1, 5, 25] as

$$\begin{cases} \mathbf{w}_k(i+1) = \mathbf{P}[\mathbf{w}_k(i) - \mu z^H(i) \mathbf{X}_k(i)] + \mathbf{g} \\ \mathbf{w}_k(0) = \mathbf{g} \end{cases} \tag{29}$$

where μ is the step size parameter, $z(i) = \mathbf{w}_k^H(i) \mathbf{X}_k(i)$, $\mathbf{P} = \mathbf{I} - \mathbf{c}_k (\mathbf{c}_k^H \mathbf{c}_k)^{-1} \mathbf{c}_k^H$ and $\mathbf{g} = \mathbf{c}_k (\mathbf{c}_k^H \mathbf{c}_k)^{-1} \mathbf{f}_k$.

Using (28) or the iteration algorithm in (29), the adaptive weight vectors of the K non-uniform sub-bands can be obtained, and they can be used to obtain the K output data on non-uniform frequencies. Then, to obtain the temporal-domain signal, the data of non-uniform frequencies is processed by the non-uniform inverse discrete Fourier transform (NIDFT), which requires the direct inverse computation of the Vandermonde matrix with large order K. However, as discussed in [24], the Vandermonde matrix is usually ill-conditioned for large order K, and a direct inverse computation is not reliable. Therefore, those data of K non-uniform frequencies cannot be processed by a direct inverse computation, and thus the time-domain output of the beamformer cannot be obtained. In addition, the computational complexities of matrix inversion and matrix multiplication are high computational burden in practice.

In this section, a new method is presented to recover the residual adaptive vectors. As illustrated in Fig. 3, the optimum weight vectors are input to the adaptive weight analysis module to recover the adaptive weight vectors of all N sub-bands. In **Algorithm 2**, the method to recover adaptive weight vectors is given.

Algorithm 2 Adaptive weight analysis module

1: Initialize: $n = 1$;

2: If $\frac{|\tilde{f}_n - f_k|}{f_k} \leq \Delta B$, $k = 1, 2, ..., K$, calculate adaptive weight vector of the frequency $\tilde{f}_n$ as

$$\mathbf{w}_n = \mathbf{w}_k \tag{30}$$

or

$$\mathbf{w}_n = \mathbf{w}_k{}^{\circ} \tilde{\mathbf{w}}_{n,k} \tag{31}$$

where

$$\tilde{\mathbf{w}}_{n,k} = [e^{-j2\pi(f_k - \tilde{f})\tau_1(\theta_0)}, e^{-j2\pi(f_k - \tilde{f})\tau_2(\theta_0)}, ..., e^{-j2\pi(f_k - \tilde{f})\tau_M(\theta_0)}]^T \tag{32}$$

3: $n = n + 1$. If $n > N$, end loop; Else, jump to the step 2.

In Step 2 of **Algorithm 2**, two methods are given to refactor the all N adaptive weight vectors. In (30), if $\frac{|\tilde{f}_n - f_k|}{f_k} \leq \Delta B$, it means that the frequency $\tilde{f}_n (n = 1, 2, ..., N)$ is in the k-th sub-band, whose centre frequency is f_k. In the NUDM, if the adaptive weight vector of $\tilde{f}_n$, $\mathbf{w}_n$, is equal to $\mathbf{w}_k$, which can cause look direction errors. Since the frequency $\tilde{f}_n$ and f_k meet the RBM, the look direction error is less than the minimum half of 3dB beamwidth of the passband frequency, which implies that look direction error is acceptable. Moreover, the proposed approach adds no extra computational complexity.

In the second method, (31), $\circ$ is the Hadamard product, and $\tilde{\mathbf{w}}_{n,k}$ is the correction factor, which is used to compensate for the effect of misalignment between $\tilde{f}_n$ and f_k. In most cases, $\tilde{f}_n \neq f_k$. If $\mathbf{w}_n$ is equal to $\mathbf{w}_k$, as discussed above, there will be a small look direction error on frequency $\tilde{f}_n$. Thus, the correction factor, $\tilde{\mathbf{w}}_{n,k}$, is used to reduce the look direction error caused by the misalignment between $\tilde{f}_n$ and f_k. However, the correction factor may make the nulls of the interference malformed and affect the anti-interference capability. In addition, compared with (30), the calculations in (31) are more computationally intensive in refactoring all N adaptive weight vectors. The simulations of the FNUD-SAB with (30) and (31) will be given in Section 5, and the performance of two approaches in broadband beamforming will be shown and discussed.

Since the proposed FNUD-SAB using the NUDM has fewer sub-bands, the proposed beamformer has lower computational complexity than the conventional UD-SAB. Moreover, **Algorithm 1** can be implemented offline, and the frequency selection modules only need to save the frequency, which is used to calculate the adaptive weights. Since **Algorithm 1** and **Algorithm 2** with (30) have no extra calculation in real-time, FNUD-SAB with (30) does not add any extra computational complexity. In addition, as discussed in[23], the acceptable pointing error should be in the range of the half-power beamwidth (3dB beamwidth), the proposed FNUD-SAB uses **Algorithm 1** and **Algorithm 2** with (30) to make sure that the pointing error is less than the lowest half-power beamwidth of the passband in each sub-band as proved in (13) and (14). Therefore, the proposed adaptive broadband beamformer yields satisfactory performance as the conventional SAB with less computational complexity.

5. Simulation Results

In presenting several simulation studies to demonstrate the benefits of the proposed approach, we use the conventional UD-SAB as the baseline for comparison. Our simulation scenario comprises the following setup: Number of ULA antennas M: 50; One broadband SOI comes from θ_0 direction $-5°$, and one broadband interference signal is from $35°$; The lowest frequencies of the two signals are 300 MHz; The frequency bands of the two signals are 1.25 GHz; The signal-to-interference ratio (SIR) and interference-to-noise ratio (INR) are assumed as -40 dB and 40 dB, respectively; The adaptive iterative algorithm introduced in (29) is used to obtain the adaptive weights; and the step size parameter μ is 1×10^{-8}.

As the number of ULA antennas M is obtained, the relative bandwidth ΔB and the common ratio q can be obtained. Then, as the lowest frequency of the passband is given out, the boundary frequency $\bar{f}_1$ of the 1st sub-band can be obtained by (20). Then, the 1st bandwidth can be obtained. As said in Section 3 and shown in the Fig. 2, the minimum absolute bandwidth, i.e., the 1st bandwidth, is used to split the passband in the

conventional UDM. Through the calculation, the UD-SAB needs 202 sub-bands. However, the FNUD-SAB needs only 103 sub-bands through **Algorithm 1**. In the Section 3, the number of non-uniform sub-band, which using NUDM with NDFT, is given out as $\left\lceil \log_q^{\frac{f_{\max}}{f_{\min}}} \right\rceil = 81 < 103$. Strictly, although the **Algorithm 1** is NUDM-based, it is still based on the uniform DFT. It is worth noticing that the FNUD-SAB using **Algorithm 1** needs larger number of the sub-bands than the NUDM with NDFT. However, the NDFT is ill-conditioned for a large number of elements [24]. And hence, the **Algorithm 1** is an effective way for broadband beamforming with less number of sub-bands than the UDM.

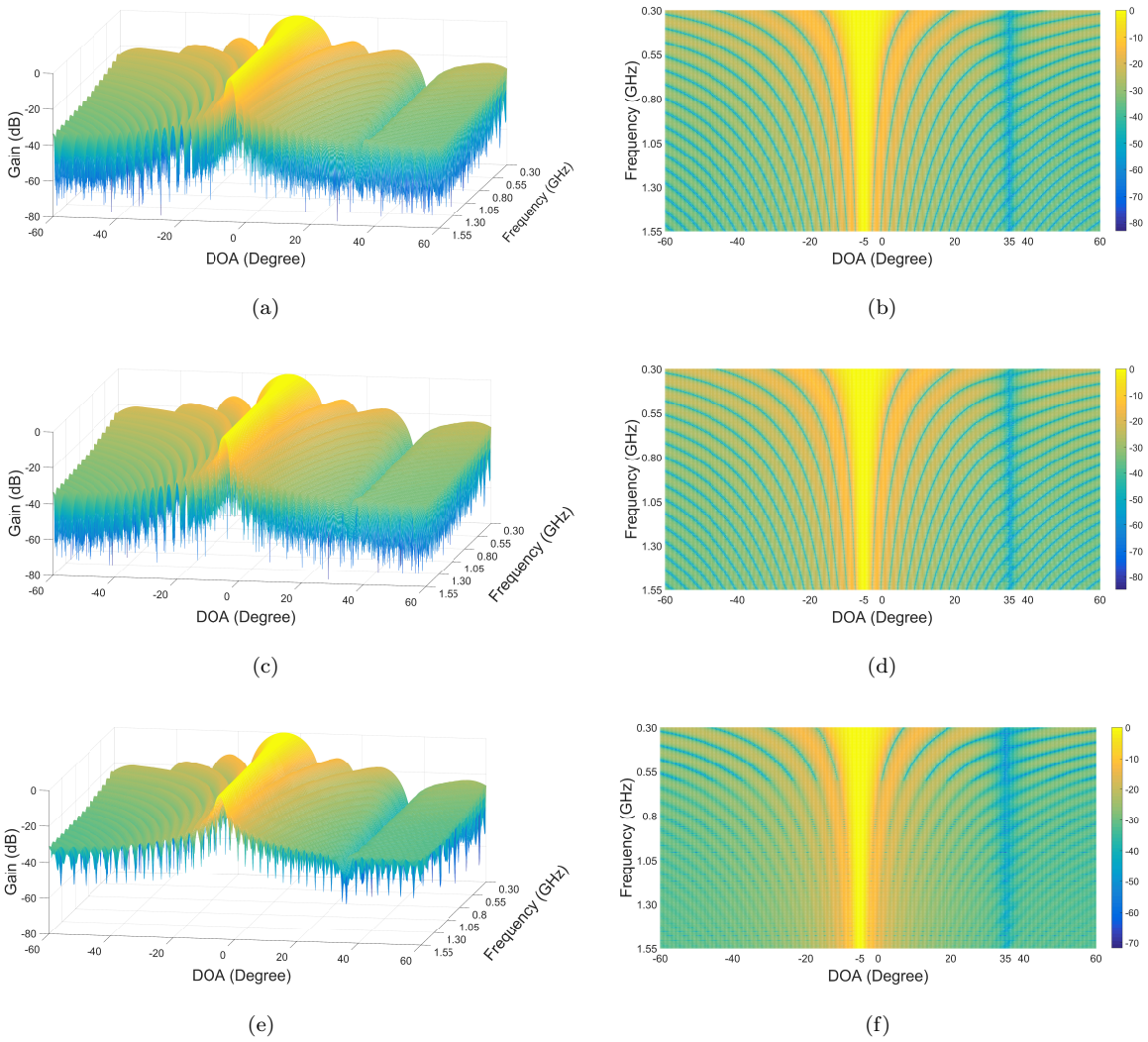

Figure 4: Beam patterns and their vertical views of (a) and (b) conventional UD-SAB; (c) and (d) FNUD-SAB with (30); (e) and (f) FNUD-SAB with (31).

Fig. 4 shows the beam patterns and their vertical views from the conventional and proposed approaches. The accuracy of the DOA is 0.1°. Comparing Fig. 4(c) and 4(e) with 4(a), one can see that the proposed algorithms yield satisfactory beam pattern shapes. From Fig. 4(b), 4(d) and 4(f), one can see that the proposed beamformers, FNUD-SAB with (30) and (31), produce undistorted response to the SOI and effectively restrain the nulls to the interference as well as the conventional UD-SAB. As discussed in Section 3, the minimum absolute

bandwidth is the first sub-band of the passband and should be satisfied in the UDM and NUDM to ensure the look direction error in the range of the half-power beamwidth. In passband, the conventional UD-SAB using UDM needs 202 sub-bands, whose received data are used to calculate the adaptive weights. However, the proposed FNUD-SAB using **Algorithm 1** needs only 103 sub-bands in the passband. Therefore, from the beam patterns, one can see that the proposed FNUD-SAB yields satisfactory performance in beam patterns with almost 50% of the computational complexity of the conventional UD-SAB. For a large-scale ULA, e.g., $M = 50$, the proposed FNUD-SAB significantly reduces the computational burden, and hence should lead to substantial performance gains.

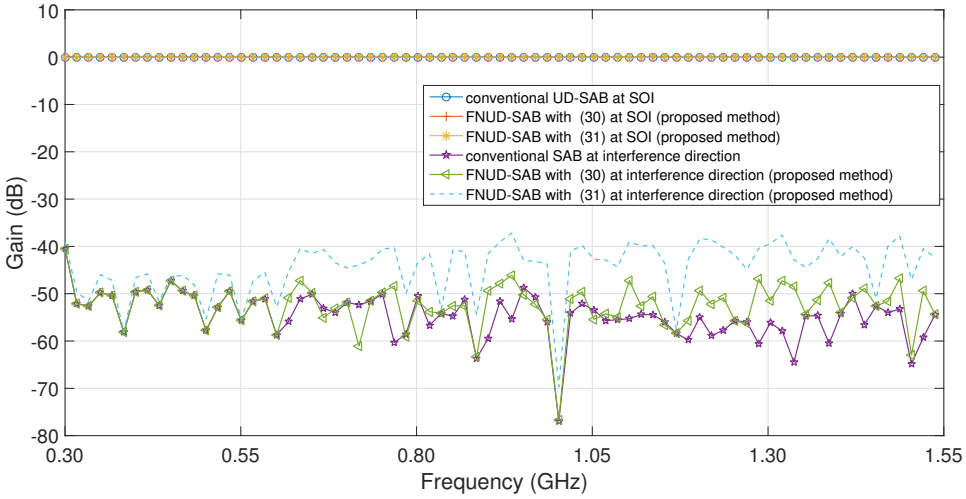

Figure 5: Frequency response of conventional UD-SABs and proposed beamformers to the SOI and interference direction (cross-sections of Fig. 4), where the SOI and interference direction are from -5° and 35°, respectively.

In Fig. 5, the magnitude of the frequency responses of the algorithms at the desired and interference directions are illustrated. The figure illustrates that the proposed FNUD-SAB with (30) or (31) has a flat response for the desired direction and deep nulls for the interference direction similar to the conventional UD-SAB. Response of the proposed algorithm to the SOI is flat and equal to 0 dB, which means that the proposed method has a satisfactory look direction response. The nulls of the proposed method with (30) to the interference is almost the same as the conventional method. However, the null of the proposed method with (31) to the interference is not as deep as the other two methods. This phenomenon is caused by the corrected factor $\tilde{\mathbf{w}}_{n,k}$ in (31). The corrected factor revises the look direction errors; however, it also affects the performance in terms of anti-interference. Therefore, the corrected factor does not always make the response to the SOI better obviously, on the contrary, it makes the performance on anti-interference more terrible than the proposed method without the corrected factor.

Fig. 6 illustrates the evolution of the output signal-to-interference-plus-noise ratio (SINR) for the conventional and the proposed methods obtained by averaging over 100 Monte Carlo analyses. The convergence rate of the proposed method with (30), which has 103 sub-bands in the passband, is the same as the convergence rate of the conventional method with 202 sub-bands in the passband. The output SINR of the proposed method with (30) is only 0.83 dB less than that of the conventional method using 202 sub-bands. However, the computational

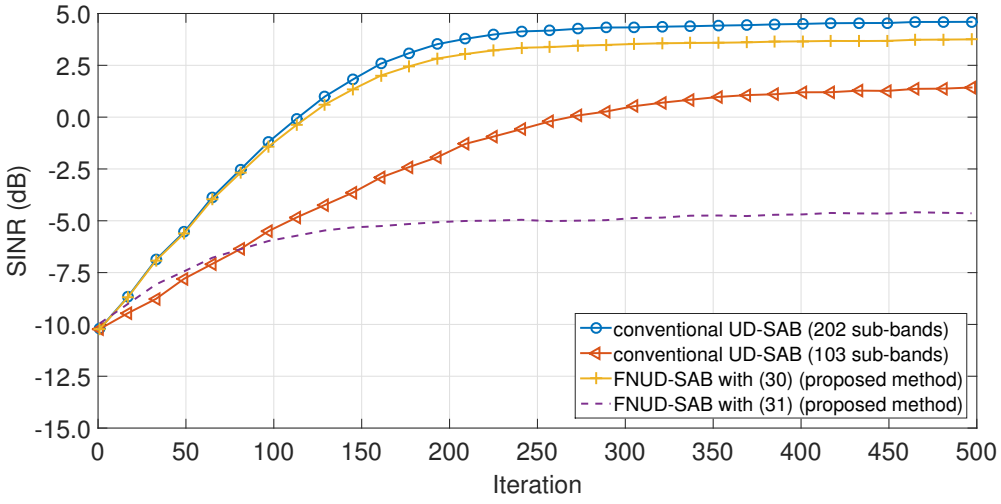

Figure 6: Evolution of output SINR for the conventional UD-SABs and proposed beamformers with 100 Monte Carlo analyses.

complexity of the proposed method is nearly 50% of the conventional method using 202 sub-bands without any other extra computation. If the conventional method uses 103 sub-bands in the pssband, it will have the same complexity as the proposed method; however, the output SINR of conventional method will be 2.61 dB less than that of the proposed method with (30), and 3.44 dB less than that of the conventional method using 202 sub-bands. Compared with conventional UD-SAB (103 sub-bands), the proposed FNUD-SAB with (30) has the same computational complexity in circulating the adaptive weight vectors, but it has the better performance on output SINR. Since the FNUD-SAB with (30) (proposed method) has the longer equivalent tapped delay-line length than the conventional UD-SAB, the proposed method with (30) yields better output SINR with the same computational complexity compared with the conventional method (103 sub-bands).

Fig. 6 also illustrates that the proposed method with (31) has the worst output SINR. As discussed earlier, the correction factor revises the look direction errors, however, it also affects the anti-interference performance. Therefore, the correction factor does not always make the response to the SOI better, on the contrary, it makes the performance on anti-interference more terrible than the proposed method without the corrected factor. In addition, the proposed method with (31) adds extra computational complexity to refactor the adaptive weights. For the proposed method with (30), the extra computational complexity is not necessary. Therefore, the proposed FNUD-SAB with (30) has lower computational complexity but better broadband beamforming performance compared with the FNUD-SAB with (31), thus the proposed method with (30) is appropriate for the real-time applications.

We evaluated these algorithms (MATLAB-based) on a system with a 2.7 GHz i7-6820HQ processor with 32GB memory. Since the scale of the antenna is constant, the data scale of each sub-band is the same, leading to same computational time for each sub-band. In our study, we found that the computational time for a single sub-band, with 100 Monte Carlo runs, is approximately 35 seconds or 350ms for single sub-band per run. Using this as a metric, for a conventional UD-SAB with 202 sub-bands, this would require approximately 350ms $\times 202 =$ 71 seconds. In contrast, for the proposed FNUD-SAB approach, this would require only 350ms $\times 103 = 36$ seconds. Furthermore, if the sub-bands are run concurrently (using multiple threads), assuming negligible thread overheads,

this would require only 350ms. However, the proposed FNUD-SAB has the lower computational complexity with a satisfactory performance on the output SINR.

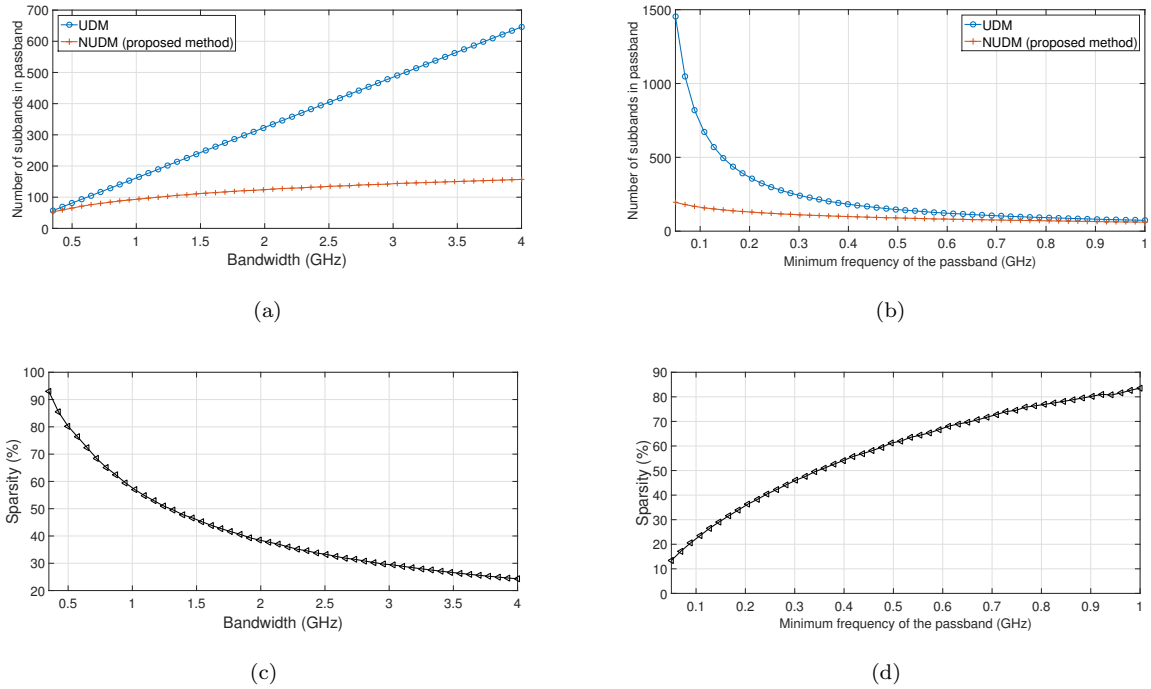

Figure 7: Number of sub-bands in the passband for different (a) bandwidth. (b) minimum frequency of passband. Sparse rate for different (c) bandwidth. (d) minimum frequency of passband.

Fig. 7 shows the number of sub-bands in the conventional UDM and the proposed NUDM in **Algorithm 1** with different bandwidth and minimum frequency of the passband. In Fig. 7(a) and 7(c), the numbers of sub-band and sparsity rates are plotted over different bandwidth but with the same minimum frequency of the passband at 0.3 GHz. The sparsity rate is defined as the number of sub-bands in the proposed NUDM divided by the number of sub-bands in the conventional UDM. When the bandwidth is larger than 1.25 GHz, the number of sub-bands in the conventional UDM is much larger than that of the proposed NUDM, and the sparsity rate is less than 50%. That is, with the increase in the bandwidth, the proposed NUDM has much less computational complexity than the conventional UDM. In Fig. 7(b) and 7(d), the numbers of sub-bands and sparsity rates are plotted over different minimum frequency of the passband but with the same bandwidth at 1.5 GHz. When the minimum frequency is less than 0.35 GHz, the number of sub-bands of the conventional UDM is much larger than that of the proposed NUDM, and the sparsity rate is less than 50%. That is, with the decrease in the minimum frequency, the proposed NUDM has much less computational complexity than the conventional UDM. From Fig. 7, one can see that the proposed NUDM has much less computational complexity than the conventional UDM. When the minimum frequency is low and the bandwidth is wide, the advantage of the proposed method is more pronounced.

When comparing the ABR values, as highlighted before, for UDM, the ABR is equal to 1. For the case of NUDM, the ABR is equal to $q = \left(\frac{2+\Delta B}{2-\Delta B}\right) = \left(\frac{2+\frac{5.56}{\sqrt{3}\pi M}}{2-\frac{5.56}{\sqrt{3}\pi M}}\right) = 1.02065$. When the passband bandwidth is the same,

the method, whose ABR is much larger than 1, has the lowest number of sub-bands, i.e., the lowest computational complexity.

As previously stated, the FNUD-SAB using the NUDM is still based on the uniform DFT. Find a feasible technology to directly split the passband into the non-uniform sub-bands and transform the non-uniform frequency-domain signal back to the time-domain signal without distortion are the further research works.

6. Conclusions

In this paper, we presented a computationally efficient, non-uniform decomposition-based approach to beamforming. To render the proposed non-uniform domain decomposition method, we proposed a relative beamwidth method. We proved that the relative bandwidth of a sub-band is invariant to the center frequency of the sub-bands and in fact a constant. Consequently, we proved that when performing the non-uniform domain decomposition, the center frequencies of sub-bands follow a geometric progression, whose ratio value is greater than one. As such, for a given passband, the proposed non-uniform decomposition method results in fewer sub-bands than the number of sub-bands resulting from the conventional uniform domain decomposition method. We then presented a FNUD-SAB and its adaptive variant based on the NUDM. We showed that the new beamformer has lower computational complexity than the conventional UD-SAB and its broadband beamforming performance is comparable to that of the UD-SAB. Moreover, the non-uniform frequencies can be obtained offline, and the frequency selection modules need to save only the frequencies that are used to calculate the adaptive weights. Using practically-driven simulations, we demonstrated the effectiveness of the proposed approach both in terms of computational complexity, and in terms of runtime performance.

Acknowledgment

This work was supported in part by the National Natural Science Foundation of China under Grants 61501240, 61471196 and 61401207, by the Key Projects Foundation of Shanghai Aerospace under Grant SAST201437, by the State Scholarship Fund of the China Scholarship Council (CSC), and by the College Graduate Scientific Research Innovation Fund in Jiangsu Province of China under Grant KYZZ16_0187.

References

[1] W. Liu, S. Weiss, Wideband beamforming: concepts and techniques, Vol. 17, John Wiley & Sons, 2010.

[2] C. Sun, Handbook on advancements in smart antenna technologies for wireless networks, IGI Global, 2008.

[3] S. Nordholm, H. H. H. Dam, C. C. Lai, E. Lehmann, Broadband beamforming and optimization, in: Academic Press Library in Signal Processing Volume 3Array and Statistical Signal Processing, Elsevier, 2014, pp. 553–598.

[4] M. Crocco, A. Trucco, A computationally efficient procedure for the design of robust broadband beamformers, IEEE Transactions on Signal Processing 58 (10) (2010) 5420–5424.

[5] O. L. Frost, An algorithm for linearly constrained adaptive array processing, Proceedings of the IEEE 60 (8) (1972) 926–935.

[6] R. Gooch, J. Shynk, Wide-band adaptive array processing using pole-zero digital filters, IEEE transactions on antennas and propagation 34 (3) (1986) 355–367.

[7] H. Duan, B. P. Ng, C. M. See, A new broadband beamformer using iir filters, IEEE Signal Processing Letters 12 (11) (2005) 776–779.

[8] H. Duan, B. P. Ng, C. M. S. See, J. Fang, Broadband beamforming using tdl-form iir filters, IEEE Transactions on Signal Processing 55 (3) (2007) 990–1002.

[9] S. R. Seydnejad, R. Ebrahimi, Broadband beamforming using laguerre filters, Signal Processing 92 (4) (2012) 1093–1100.

[10] W. Liu, R. J. Langley, An adaptive wideband beamforming structure with combined subband decomposition, IEEE Transactions on Antennas and Propagation 57 (7) (2009) 2204–2207.

[11] S. Zhang, W. Sheng, Y. Han, X. Ma, Generalised reduced-rank structure for broadband space–time gsc and its fast algorithm, Signal Processing 133 (2017) 117–121.

[12] S. Zhang, W. Sheng, X. Ma, Y. Han, R. Zhang, Low-complexity space-time processing for wideband beamforming, in: 2016 IEEE International Symposium on Phased Array Systems and Technology (PAST), IEEE, 2016, pp. 1–5.

[13] B. Sällberg, Faster subband signal processing [dsp tips&tricks], IEEE Signal Processing Magazine 30 (5) (2013) 144–150.

[14] J. Khalab, M. Ibrahim, Novel multirate adaptive beamforming technique, Electronics Letters 30 (15) (1994) 1194–1195.

[15] F. Lorenzelli, A. Wang, D. Korompis, R. Hudson, K. Yao, Subband processing for broadband microphone arrays, The Journal of VLSI Signal Processing 14 (1) (1996) 43–55.

[16] Y. Zhang, K. Yang, M. G. Amin, Adaptive array processing for multipath fading mitigation via exploitation of filter banks, IEEE Transactions on antennas and propagation 49 (4) (2001) 505–516.

[17] E. Chau, H. Sheikhzadeh, R. Brennan, T. Schneider, A subband beamformer on an ultra low-power miniature dsp platform, in: Acoustics, Speech, and Signal Processing (ICASSP), 2002 IEEE International Conference on, Vol. 3, IEEE, 2002, pp. III–2953.

[18] J. M. de Haan, N. Grbić, I. Claesson, S. Nordholm, Design and evaluation of nonuniform dft filter banks in subband microphone arrays, in: Acoustics, Speech, and Signal Processing (ICASSP), 2002 IEEE International Conference on, Vol. 2, IEEE, 2002, pp. II–1173.

[19] W. Neo, B. Farhang-Boroujeny, Robust microphone arrays using subband adaptive filters, IEE Proceedings-Vision, Image and Signal Processing 149 (1) (2002) 17–25.

[20] W. Liu, S. Weiss, Frequency invariant beamforming in subbands, in: Signals, Systems and Computers, 2004. Conference Record of the Thirty-Eighth Asilomar Conference on, Vol. 2, IEEE, 2004, pp. 1968–1972.

[21] Y. Zhang, K. Yang, M. G. Amin, Subband array implementations for space-time adaptive processing, EURASIP Journal on Applied Signal Processing 2005 (2005) 99–111.

[22] W. Liu, R. Langley, Adaptive wideband beamforming with combined spatial/temporal subband decomposition, PIERS Online 3 (7) (2007) 991–996.

[23] W.-D. Wirth, Radar techniques using array antennas, Vol. 10, IET, 2001.

[24] S. K. Mitra, Digital signal processing: a computer-based approach, McGRaw-Hill, 2001.

[25] F. Huang, W. Sheng, X. Ma, W. Wang, Robust adaptive beamforming for large-scale arrays, Signal Processing 90 (1) (2010) 165–172.